Comparison of measured and calculated scattering from surface aerosols with an average, a size-dependent, and a time-dependent refractive index

Yong Cai,[1] Derek C. Montague,[1] and Terry Deshler[1]

Received 9 June 2010; revised 13 October 2010; accepted 26 October 2010; published 20 January 2011.

[1] Midcontinental surface aerosols have been measured at a small, minimally polluted city in summer and winter and on a nearby remote mountain in summer. Aerosol scattering, absorption, size distribution, and composition were measured using a three-wavelength nephelometer, an aethalometer, a passive cavity aerosol spectrometer, a scanning mobility particle sizer, an Aerodyne quadrupole aerosol mass spectrometer, and conventional filter systems. Size-dependent, time-dependent, and averaged refractive indices are estimated from the aerosol composition measurements and then used to calculate time-dependent aerosol scattering. The calculated scattering values show differences that are generally less than 5% on average for all three refractive indices, suggesting that the average refractive index is adequate for scattering estimations from time- or size-dependent aerosol measurements. The calculated scattering (backscattering) at 550 nm ranges from 2% less to 23% greater (11–22% smaller) than that measured. These differences decrease at 450 nm and increase at 700 nm and significantly exceed these values if optical size distribution measurements are not corrected for an appropriate index of refraction. Optimal agreement between calculated and measured scattering is achieved on 4 of the 6 days investigated in detail, if the real refractive index of the aerosol organic species ranges from 1.45 ± 0.02 at 450 nm to 1.62 ± 0.05 at 700 nm. Single-scatter albedos are also calculated and found to be in good agreement with those derived from the experimental observations, ranging from 0.79 to 0.87 in the city and constant, near 0.95, on the mountain top.

Citation: Cai, Y., D. C. Montague, and T. Deshler (2011), Comparison of measured and calculated scattering from surface aerosols with an average, a size-dependent, and a time-dependent refractive index, *J. Geophys. Res.*, *116*, D02202, doi:10.1029/2010JD014607.

1. Introduction

[2] Ambient aerosols have large impacts on global radiative forcing and create large uncertainties in our understanding of future climate through direct interaction with solar and terrestrial radiation and through their influences on the formation and growth of clouds and haze [*Intergovernmental Panel on Climate Change* (*IPCC*), 2007]. Understanding the interrelationships between the optical properties and physicochemical characteristics of the atmospheric aerosol is essential to improve quantitative estimates of radiative forcing and to interpret the increasing number of remotely sensed and in situ observations of atmospheric particles. Achieving agreement between calculated and measured aerosol optical properties facilitates attainment of this goal. Numerous optical closure studies of this kind have therefore been carried out in a variety of locations, from urban areas and polluted boundary layers [e.g., *Kim and Boatman*, 1990a; *Quinn et al.*, 1996; *Philippin et al.*, 1998; *Quinn and Coffman*, 1998; *Ross et al.*, 1998; *Collins et al.*, 2000a, 2000b], to broader regions [e.g., *Pesava et al.*, 2001; *Wang et al.*, 2002; *Quinn et al.*, 2004], and regions aloft [*Collins et al.*, 2000b; *Han et al.*, 2003; *Barnaba et al.*, 2007], but as yet, few have been conducted in remote continental areas minimally impacted by human activities.

[3] In comparisons of calculated and observed aerosol optical properties, calculations using Mie theory require the size, number concentration, and refractive index (RI) of the particles. Of these properties, RI is the most difficult to measure routinely with high temporal and/or spatial resolution for ambient particles. Various methods have been employed to determine visible wavelength average RI values of particle ensembles in urban, rural, and maritime locations, at the surface and aloft. These methods include iterative determinations of RI that lead to optimal agreement between measured particle size distributions obtained with a scanning mobility particle sizer (SMPS) and an optical particle counter (OPC) [e.g., *Hand and Kreidenweis*, 2002; *Guyon et al.*, 2003], a comparison of measured lidar back-

[1]Department of Atmospheric Science, University of Wyoming, Laramie, Wyoming, USA.

0148-0227/11/2010JD014607

scatter signals [*Redemann et al.*, 2000; *Deshler et al.*, 2000] or total scattering [*Liu and Daum*, 2000] with those calculated using observed in situ size distributions, deconvolution of simultaneously measured forward and back-scattered light, and calculation of RI from the volume averaged chemical composition of the particles [e.g., *Horvath*, 1998; *Ebert et al.*, 2004; *Schkolnik et al.*, 2007; *Cook et al.*, 2007]. Average RI values derived by these methods typically range from 1.33 to 1.57 for the real component of the index and are sensitive to measurement location and prevailing relative humidity. Few measurements have focused on the determination of size- or time-dependent RIs [*Lowenthal et al.*, 2000; *Pesava et al.*, 2001]. Comparison of aerosol scattering calculated using time-dependent, size-dependent, and averaged RI values allows the potential advantages of conducting highly resolved measurements to be assessed when estimating the impact of tropospheric aerosol on the Earth's radiation balance. Similarly, these comparisons may also be helpful in understanding field aerosol observations.

[4] In this paper we report surface observations of aerosol scattering and absorption, together with relevant size distribution and composition information, at two sites in southeastern Wyoming. Measured aerosol scattering values at three wavelengths are compared with calculated scattering based on size distribution and aerosol composition measurements, using time-resolved, size-resolved, and average RIs. All three RIs are derived from filter, aethalometer, and aerosol mass spectrometric measurements. The sensitivity of calculated scattering to variations in these RI values is investigated, particularly with regard to that of the organic component of the aerosol, to assess the accuracy to which RI must be known to obtain realistic estimates of aerosol scattering from size distribution information.

2. Sampling Conditions and Instruments

[5] Ambient aerosol measurements were carried out continuously for a total of three 2 week long periods at two sites in southeastern Wyoming, with occasional short period data loss due to instrumental problems. Sampling was conducted in Laramie (LAR) during summer, 20 July 2005 to 4 August 2005, and winter, 12–26 February 2006, and for a third period at our nearby mountain top observatory on Elk Mountain (EMO) during summer, 29 July 2006 to 8 August 2006 and 4–6 September 2006. Both sites are in the mountain time zone, where local time lags UTC by 7 h in winter and 6 h in summer. UTC dates and times are reported here.

[6] Laramie (41.3°N, 105.6°W, elevation 2200 m) has about 27,000 inhabitants and no large industry. During summer sampling periods, temperatures varied from 7 to 32°C, and ambient relative humidity (RH) was normally below 40% except during relatively infrequent rainstorms. In winter, temperatures were −26 to 6°C, while RH ranged between 20% and 90%. Aerosols in Laramie were sampled from a laminar flow 7.3 cm diameter vertical metal inlet extending 2 m above the roof of the seven-story engineering building at the University of Wyoming. Thus, the inlet was approximately 30 m above the ground. The aerosol instruments were in a laboratory on the top floor of the building.

[7] Elk Mountain (41.6°N, 106.5°W, elevation 3320 m) is an isolated peak to the northwest of the Medicine Bow Mountains in the northern front range of the Rocky Mountains. Summer temperatures ranged from 2°C to 23°C, and RH was generally below 40%. Aerosols were again sampled through a laminar flow 7.3 cm diameter vertical inlet extending 10 m above the surface. The inlet system was warmed as necessary to keep the sample RH below 25% in both locations, but its temperature was never allowed to exceed 30°C. The low RH ensured that the sampled aerosols were essentially composed of dry particles with minimal growth due to water uptake. Continuous night and day sampling was carried out at each location, throughout the measurement campaigns.

[8] A block diagram of the configuration of the instruments is shown in Figure 1. The sample inlet flow was simultaneously directed to four primary sampling lines for measurements of aerosol size distribution, scattering, absorption, and composition. Attached to line 1 was a passive cavity aerosol spectrometer probe (PCASP-100, 0.11–3.15 μm, PMI, Inc.), a static thermal gradient cloud condensation nuclei (CCN) counter (University of Wyoming) [*Snider and Brenguier*, 2000; *Delene and Deshler*, 2000], and an aerodynamic particle sizer (APS, 0.52–20 μm, TSI Model 3321). Attached to line 2 were two parallel 47 mm diameter filter pack pairs, designed to provide concentration measurements of carbonaceous material, soluble ionic species, and metallic elementary cationic components of the aerosol. Attached to line 3 was a 1.0 μm cutoff cyclone upstream of two more identical, parallel filter pack pairs, and, on a separate branch, two single-wavelength (530 nm) nephelometers (Radiance Research, M903) connected in tandem but separated by a humidifier. Attached to line 4 was a 2.5 μm cutoff cyclone upstream of a three-wavelength nephelometer (TSI Model 3563), an aethalometer (Magee Scientific AE-16) [*Hansen et al.*, 1984], a scanning mobility particle sizer (SMPS, 0.016–0.76 μm, TSI Model 3936), two condensation particle counters (TSI CPC 3010 and CPC3025A), and a quadrupole aerosol mass spectrometer (QAMS, Aerodyne, Inc., 0.04–1.0 μm). An ultrahigh sensitivity aerosol spectrometer (UHSAS, 0.06–0.8 μm, PMI, Boulder, CO) was also deployed, but only at EMO. A polonium-210 charge neutralizer (not shown) was included upstream of the sampling branch leading to the QAMS and particle concentration and sizing instruments. Conductive sampling lines were used throughout, and wherever possible, the line lengths were minimized to limit diffusional losses. For instruments without internal pumps, critical orifices were used to control flow rates. Sample temperature and relative humidity were monitored in both lines 3 and 4.

3. Measurements

3.1. Refractory Species: Black Carbon and Minerals

[9] Comparisons of measured scattering extinctions with those calculated by Mie theory require RI values for the ambient particles, estimated from particle composition. Black carbon (BC) mass concentration is derived from aethalometer measurements of light absorption at 880 nm as an integrated value over all particle sizes less than 2.5 μm. Recently, *Collaud Coen et al.* [2010] have evaluated algorithms to correct aethalometer measurements due to multiple scattering, filter loading, and other smaller corrections. The correction for multiple scattering, which reduces the derived

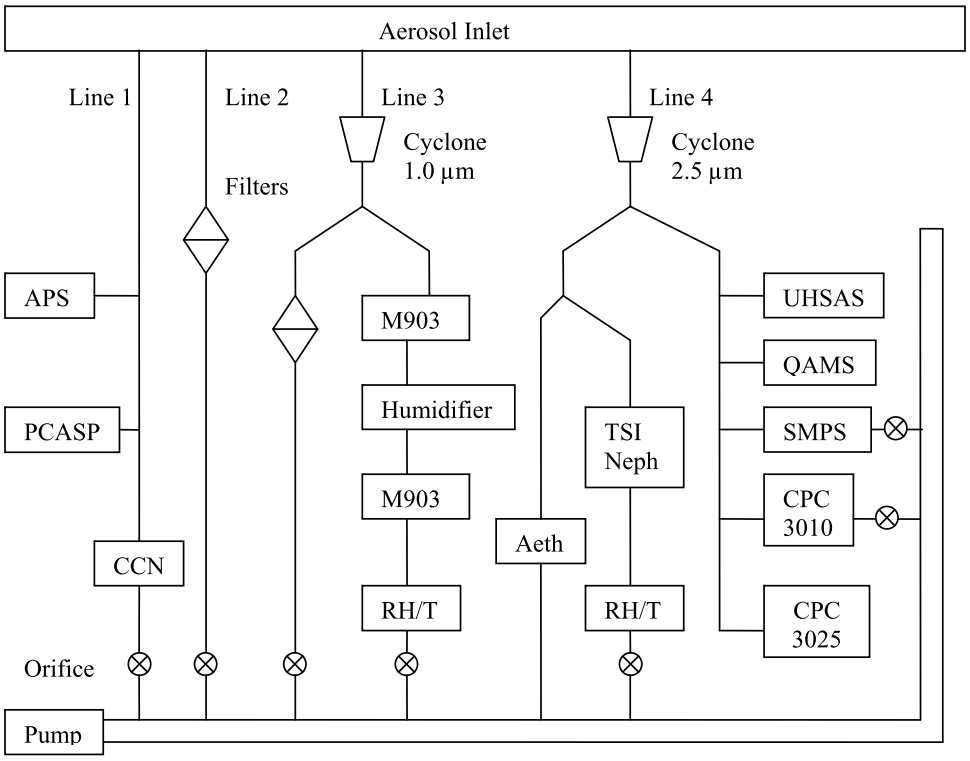

Figure 1. Block diagram of aerosol sampling system.

BC mass loading, is invariably the greatest, exceeding the second most important correction factor, filter loading ("shadowing"), which increases BC mass. The correction for shadowing is straightforward, as long as relevant attenuation measurements are recorded, although the proposed methods [*Weingartner et al.*, 2003; *Arnott et al.*, 2005; *Schmid et al.*, 2006; *Virkkula et al.*, 2007] lead to different shadowing correction factors. The correction for multiple scattering, however, requires simultaneous measurements of the aerosol absorption coefficient by an alternative method, otherwise the multiple scattering correction factor (C_{ref}) can only be estimated. Since BC mass loading is inversely proportional to C_{ref}, inaccuracies in C_{ref} lead directly to a corresponding uncertainty in BC. Reported C_{ref} values vary by more than a factor of 2 and are site dependent [*Collaud Coen et al.*, 2010].

[10] Unfortunately, independent absorption coefficient measurements are not available in this study, so multiple scattering corrections cannot be definitively carried out. Thus, although the shadowing correction can be estimated, the overall correction factor may reduce the uncorrected BC mass by as much as a factor of 2, depending on the chosen value of C_{ref}. Since it is not possible to define the overall correction factor precisely, uncorrected BC mass will be used for our calculations, adding appropriate uncertainties when BC mass is important for the calculation. Because BC contributes minimally to overall particulate mass, this approach does not affect derived particle density and real RI values significantly.

[11] Before BC can be combined with the mass loadings of the other particulate species, it is necessary to assign it a size distribution. Previous measurements suggest that ambient BC mass loadings generally exhibit a strong accumulation mode peak at aerodynamic diameters from 0.1 to 0.6 μm [*Hitzenberger and Tohno*, 2001; *Viidanoja et al.*, 2002; *Clarke et al.*, 2004; *Schwartz et al.*, 2008a, 2008b; *Stratmann et al.*, 2010]. In this study, most SMPS measured volume size distributions can be fit well with a lognormal function peaked at mobility diameters from 0.2 to 0.4 μm. Without additional information, we approximate the measured BC with a lognormal size distribution with median diameter and distribution width given by the SMPS volume size distribution and total mass concentration given by the aethalometer data. Implicit in this approach is the assumption that the BC contribution to supermicrometer particles is negligible. The sensitivity of calculated scattering to the size distribution chosen for BC is discussed subsequently.

[12] Filter samples, collected over periods from 24 to 72 h, were analyzed by X-ray fluorescence at the Division of Atmospheric Sciences of the Desert Research Institute, Reno, NV, (DRI) for mass loadings of elements in the aerosol [*Watson et al.*, 1999]. Principal elements detected were silicon, aluminum, and calcium, together with smaller quantities of iron, potassium, phosphorus, sodium, and traces of other metallic elements. Following conventional practice, the crustal elements are presumed to be present as species that can be represented by their common oxides [*Zhang et al.*, 1994; *Watson et al.*, 2001]. The percentage mass contributions of these species to the total particulate mass loadings averaged over the filter collection time periods are generally low for the submicrometer particles, ranging, with their standard deviations, from 3.1% ± 0.7% (summer 2006) and 5.2 ± 1.2% (summer 2005) to 9.7 ± 5.6% (winter 2006). The largest percentage contribution was 16.9%, on 23–24 February 2006. Crustal minerals dominate the composition of supermicrometer coarse mode particles, with

percentage mass contributions ranging from 63.1% on 24 February 2006 to 89.0% on 5 September 2006. Mineral mass contributions to the submicrometer particles may therefore possibly derive from the smallest particles of the coarse mode, with sizes <1 μm, that extend into the accumulation mode size regime, and if so, they would be expected to contribute primarily to the composition of the larger particles in this latter mode.

3.2. Nonrefractory Species

[13] Mass concentrations of aerosol species susceptible to flash vaporization at 590°C, the operating temperature of the QAMS vaporizer, were measured simultaneously by both filter samples and the QAMS. Water-soluble inorganic anionic species from the filters, including sulfate, were analyzed by routine ion chromatography at DRI [*Chow and Watson*, 1999], yielding mass loadings for both submicrometer and supermicrometer particles averaged over the filter sample collection time period. The QAMS measured species mass loadings with a time resolution of 5 min. Particle size-resolved concentrations were also obtained by operating the instrument in its standard alternating mass spectral (MS) and time-of-flight (TOF) modes [*Jayne et al.*, 2000; *Jimenez et al.*, 2003; *Takegawa et al.*, 2005; *Canagaratna et al.*, 2007]. The principal species measured were sulfate, nitrate, ammonium, and organics. The measurements suggest that sufficient ammonium is present to convert all observed nitrate and sulfate to their fully ammoniated salts.

[14] For calculation of RIs, mass loadings of the species measured by the QAMS must first be combined with those for BC and the minerals. To do this requires that the measured mass loadings are first corrected to account for QAMS collection efficiency (CE), which is often less than unity [*Canagaratna et al.*, 2007; *Matthew et al.*, 2008]. The overall CE is believed to vary with particle size, phase, composition, and morphology, because these factors influence the transmission efficiency of the instrument's aerodynamic lens (E_L), the beam divergence of particles in the time-of-flight chamber (E_S), and the fraction of particles striking the vaporizer that volatilize (E_B) [*Huffman et al.*, 2005, *Matthew et al.*, 2008]. CE is given by the product of these three efficiencies [*Canagaratna et al.*, 2007]. Traditionally, CE has been estimated by comparing QAMS species mass loadings either with those simultaneously obtained using other mass measurement techniques [*Weber et al.*, 2001; *Takegawa et al.*, 2005; *Canagaratna et al.*, 2007], or with those calculated from measurements of the flux of particles of known size and composition either at the instrument inlet [*Matthew et al.*, 2008], or transiting the instrument time-of-flight chamber [*Cross et al.*, 2007]. In the absence of more definitive information, it is invariably assumed that the same CE value can be applied to all QAMS measured species present in an internally mixed aerosol. Furthermore, CE values are usually assumed not to vary significantly over periods of hours to days, although if the nature of the sampled ambient aerosol or the prevailing relative humidity were to change significantly, this might not be the case.

[15] For this study, we have determined averaged CE values for the sampled dry particles by comparing sulfate mass loadings, derived from filter pack measurements with those from the QAMS. Details of the analyses that permit these comparisons and of time-dependent aerosol composition and size distribution are the subject of work in progress. Of relevance here are time-averaged CE values obtained for each of the 14 filter exposure time periods (24–72 h). For the days investigated here, these CE values range from 0.38 to 0.59 and allow particle size-dependent CE values to be determined, according to the method described below.

[16] Of the three efficiency factors that determine CE, the influence of E_S is minimal, because beam divergence experiments show that it is essentially unity [*Huffman et al.*, 2005]. Thus, CE values are effectively determined by $E_L(d_{va})$ and $E_B(d_{va})$ (written as functions of d_{va}, the particle vacuum aerodynamic diameter). For both small (<~0.1 μm) and large (>~0.5 μm) particles, reductions in $E_L(d_{va})$ limit the maximum CE value, whereas for intermediate size particles, when $E_L(d_{va})$ is unity, $E_B(d_{va})$ determines CE. The lens transmission efficiency, $E_L(d_{va})$, of the University of Wyoming QAMS (serial number 20) has been characterized using ammonium nitrate, diethylhexyl sebacate, and sodium nitrate particles, for vacuum aerodynamic particle diameters (d_{va}) from 0.04 to 1.183 μm [*Liu et al.*, 2007]. Currently, the quantitative dependence of $E_B(d_{va})$ on ambient relative humidity (RH) and on particle phase, composition, and size is not well understood, especially for ambient particles, although it is clear that CE values are higher for liquid particles and for those composed of readily volatilized material, and at high RH [*Matthew et al.*, 2008]. The dependence of E_B on particle size is even less well understood. For simplicity, we assume here that the value of E_B is size independent. Multiplying E_B by the measured size-dependent $E_L(d_{va})$ values yields size-dependent (CE(d_{va})) values. Combining averaged CE with the measured size-dependent QAMS mass loadings allows E_B and hence CE (d_{va}) to be determined, by applying the constraint that the mass loading integrated over all particle sizes must equal that determined using the size-independent average CE obtained from the QAMS and filter mass loading comparisons. Thus,

$$\int \frac{\mathrm{MC}^i_{\mathrm{AMS}}(d_{va})}{E_L(d_{va}) \times E_B} \mathrm{d}\log(d_{va}) = \frac{1}{\mathrm{CE}} \times \int \mathrm{MC}^i_{\mathrm{AMS}}(d_{va}) \mathrm{d}\log(d_{va}), \quad (1)$$

where $\mathrm{MC}^i_{\mathrm{AMS}}(d_{va})$ is the QAMS measured size-resolved mass concentration for composition i, and CE in equation (1), is the size-independent average value. Solving (1) for E_B determines CE(d_{va}) and thus enables corrected size-dependent QAMS mass loadings to be obtained.

3.3. Measured Scattering

[17] Scattering by particles of diameter ≤2.5 μm was measured at wavelengths of 450, 550, and 700 nm by the TSI nephelometer. Figure 2 shows the temporal variations of hourly averages of scattering and backscattering at 550 nm, as directly measured by the nephelometer, for all 45 days in the three experimental periods. In LAR in summer 2005, the average scattering decreased gradually, with an average value of 12.8 ± 6.5 Mm^{-1} and a minimum value of 3 Mm^{-1}. In winter 2006, in LAR, the scattering was initially low, but increased rapidly during the late evening of 16 February 2006 (early hours of 17 February 2006 UTC, measurement

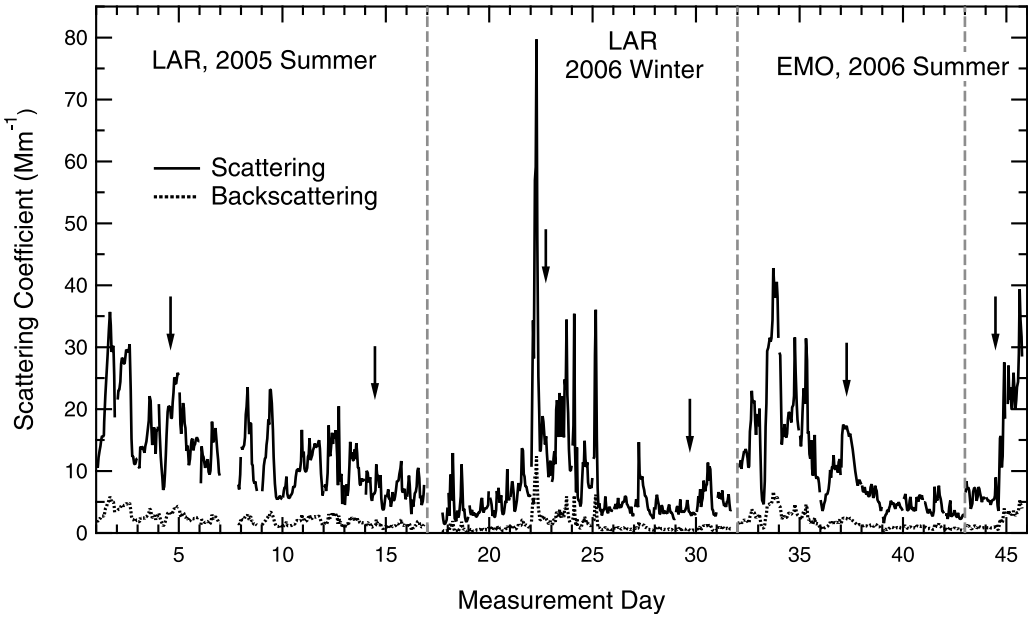

Figure 2. Hourly averaged measured scattering and backscattering at 550 nm wavelength for all 45 measurement days. The four sections separated by dashed vertical lines represent the time periods 20 July 2005 to 4 August 2005, 12–26 February 2006, 29 July 2006 to 8 August 2006, and 4–6 September 2006. Vertical arrows indicate the 6 days chosen for detailed analysis.

day 22 in Figure 2), when the overnight temperature dropped below −20°C. Scattering remained high for the following 2 days while temperatures at night stayed below −20°C. During this period the QAMS measured occasional large increases in mass loadings of the organic component of the aerosol, which probably resulted from wood smoke emitted from domestic heating sources, trapped in a poorly ventilated stable shallow surface layer. The average scattering in February 2006 was 7.7 ± 8.3 Mm^{-1}, while minimum scattering was 1.5 Mm^{-1}. At EMO, in summer 2006, the average scattering was 11.2 ± 8.7 Mm^{-1}, comparable to the summer value in LAR. This relatively high average value probably results from the regional impact of summer wildfires. For example, on 5 September 2006 (Figure 2, day 44), the sky was initially clear and average scattering was approximately 4 Mm^{-1}, but later in the day EMO was impacted by a smoke plume, causing the sky to become hazy and scattering to increase rapidly to about 30 Mm^{-1}. The non-smoke-influenced scattering values are similar to those (average value 8.6 Mm^{-1}) measured at Buffalo Pass (3224 m) in rural Colorado, 120 km southwest of LAR, and 105 km south of EMO, during the Mt. Zirkel visibility study [*Watson et al.*, 2001], and in the clean boundary layer in southwest Wyoming [*Han et al.*, 2003]. Other reported measurements [for example, *Gebhart et al.*, 2001; *Delene and Ogren*, 2002; *de Reuss et al.*, 2002; *Malm et al.*, 2005; *Vrekoussis et al.*, 2005; *Cheng et al.*, 2008; *Lyamani et al.*, 2008; *Swartzendruber et al.*, 2008; *Massoli et al.*, 2009] suggest that in the nonpolluted boundary layer, background scattering is ~5 Mm^{-1} with even lower values (~2 Mm^{-1}) aloft in the clean, free troposphere, whereas in areas affected by urban or industrial sources, scattering typically increases to 50–500 Mm^{-1} or even higher. Clearly, the low scattering values frequently observed in this study are indicative of the cleanliness of the air often experienced at both LAR and EMO.

[18] Measurements of backscatter that allow the ratio of the backscattering to total scattering coefficient, the backscatter ratio, to be determined, are important for quantitative interpretations of lidar data and for estimates of aerosol radiative forcing. Backscattering coefficients in each measurement period are approximately 1 order of magnitude smaller than those for scattering. Backscatter ratios are not significantly different for the three experimental periods, averaging 0.15 ± 0.02, 0.17 ± 0.02, and 0.22 ± 0.03 at wavelengths 450, 550, and 700 nm, respectively. Long-term climatological average backscatter ratios reported for two sites in rural Illinois and Oklahoma [*Delene and Ogren*, 2002] provide long-term comparators. At 550 nm, these backscatter ratios are ~30% lower than the average of the Wyoming measurements, 0.17 ± 0.02; however, they were calculated using scattering corrected for nephelometer truncation. Correcting for nephelometer truncation increases total scattering correction disproportionately compared to the backscattering correction. Thus, backscatter ratios are reduced [*Anderson et al.*, 1999]. Additional discrepancies with the Wyoming measurements may be due to uncharacterized differences in aerosol size distributions and/or particle compositions at LAR and EMO compared to those found in the continental Midwest.

3.4. Determination of Aerosol Refractive Index

[19] Refractive indices are estimated from collection efficiency corrected mass concentrations of ammonium nitrate, ammonium sulfate, and organic material measured by the QAMS, BC measured by the aethalometer, and

Table 1. Refractive Index and Density of Ammonium Nitrate, Ammonium Sulfate, Organic Material, Black Carbon, and Mineral Material at 550 nm Wavelength

	Ammonium Nitrate	Ammonium Sulfate	Organic Material	Black Carbon	Mineral Materials
Refractive index	1.57	1.52	1.46	1.96-0.66i	1.63-0.01i
Density (g/cm^3)	1.73	1.77	1.20	2.00	2.50

mineral material determined from the filter measurements. The daily averaged RI is calculated from daily mass concentrations of the measured submicrometer particle species. Time-dependent RI is calculated using 5 min average mass concentrations for both the material measured by the QAMS and the BC, together with daily average values for the mineral species, given by the filter samples. Size-dependent RI is calculated from the daily averaged QAMS size dependent mass concentration, the daily averaged BC distributed over the daily averaged SMPS size distribution, and the daily averaged mineral mass distributed equally over submicrometer particles >0.5 μm. Subsequently, we show that calculated scattering is minimally affected by small mass contributions of mineral species.

[20] Real RI values for submicrometer particles are calculated assuming internally mixed particle compositions using the partial molar refraction approach [*Stelson*, 1990]. The imaginary part of the complex RI is calculated by the volume weighted method [*Hasan and Dzubay*, 1983]. The densities and RIs used here for the five major contributing species to the particle composition are listed in Table 1 [*Ouimette and Flagan*, 1982; *Stelson*, 1990; *Han et al.*, 2003; *Eidhammer et al.*, 2008]. The greatest uncertainties in the tabulated values are associated with BC [*Bond and Bergstrom*, 2006] and the organics. Values for the real part of the RI of organics ranging from 1.30 [*Schkolnik et al.*, 2007] and 1.40 [*Guyon et al.*, 2003] to 1.55 [*Sloane*, 1984] have been chosen for use in scattering calculations. Given the widely varying chemical nature of organic species, it is entirely possible that all values in this range might be applicable under appropriate specific circumstances. We have selected the intermediate value (1.46) proposed by *Stelson* [1990], as our initial value, but are aware that changes in the nature of the organic material indicated by mass spectral analyses would imply that the RI of the organic component of the measured aerosol is probably not constant.

3.5. Aerosol Size Distribution and Scattering Calculations

[21] Aerosol number size distributions were measured continuously with a SMPS and a PCASP in Laramie and with a SMPS, PCASP and UHSAS at EMO. *Cai et al.* [2008] have presented detailed comparisons of size distributions measured by these instruments during these experiments. Example distributions for 3 August 2006, measured at EMO, are shown in Figure 3. Because SMPS distributions only extend up to 0.8 μm, they are used solely to define the size distributions assumed for BC, as outlined in section 3.1. The scattering calculations are based on size distributions measured by the PCASP, for particles in the range 0.11–3.15 μm. Neglecting particles in the scattering calculations smaller than 0.1 μm leads to minimal error, as particles <0.1 μm contribute <2% toward scattering [*Liu and Daum*, 2000]. Optical sizes measured by the PCASP

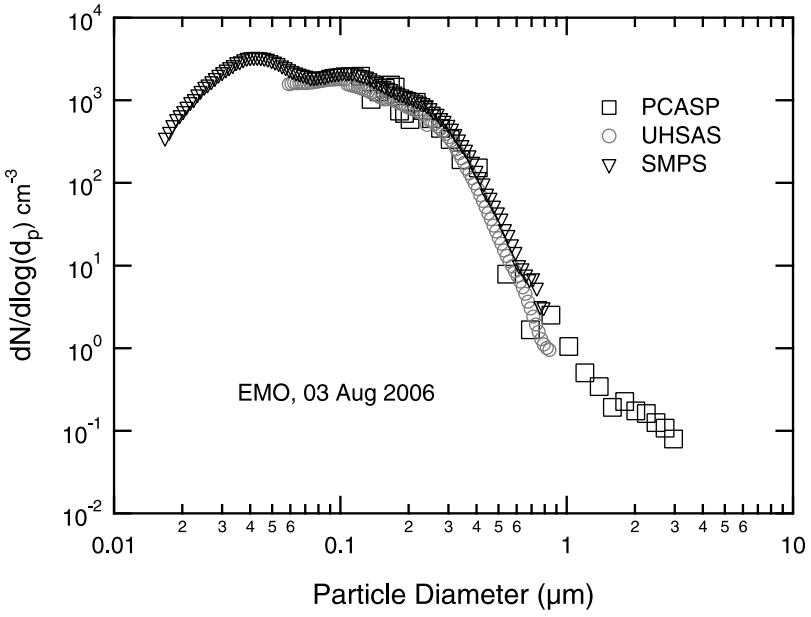

Figure 3. Number size distributions measured by the PCASP, UHSAS, and SMPS on 3 August 2006 at EMO. PCASP and UHSAS sizes are corrected using the estimated aerosol refractive index (Table 2). SMPS sizes are mobility diameter, plotted without correction.

Table 2. QAMS Collection Efficiency and Complex Refractive Index, Determined From Aerosol Composition Measurements, and Linear Regression Slopes of Fits to Calculated Versus Measured Scattering, Forced Through the Origin, for Specified Days

			Scattering			Backscattering		
	CE	Refractive Index	450 nm	550 nm	700 nm	450 nm	550 nm	700 nm
23 July 2005	0.38	1.49-0.02i	1.00	1.07	1.19	0.75	0.82	0.86
2 August 2005	0.42	1.51-0.04i	0.99	1.05	1.21	0.81	0.89	0.94
17 February 2006	0.59	1.52-0.04i	1.01	1.06	1.18	0.71	0.78	0.82
24 February 2006	0.47	1.53-0.04i	0.94	0.98	1.10	0.76	0.81	0.81
3 August 2006	0.39	1.48-0.01i	1.11	1.16	1.29	0.83	0.87	0.89
5 September 2006	0.37	1.48-0.01i	1.17	1.23	1.39	0.84	0.88	0.90

are based on calibrations with polystyrene latex (PSL) particles, for which the refractive index is 1.59-0i. Thus size distributions measured by the PCASP were corrected using the RI of the ambient particles estimated from the composition measurements (sections 3.1 and 3.2). The correction procedure is similar to that of *Liu and Daum* [2000], which extends the method of *Kim and Boatman* [1990b]. The corrected PCASP size distributions and the three types of RI are then used to calculate aerosol scattering (σ_{sca}).

$$\sigma_{sca} = \int \frac{\pi}{4} D^2 Q_{sca}(D, m) n(D) \mathrm{d}D. \quad (2)$$

Here D is the corrected particle geometric diameter, m is the refractive index, and n is the particle concentration. A Mie theory model based on the *Bohren and Huffman* [1983] Mie code is employed to correct PCASP sizes and calculate scattering efficiency Q_{sca}. Scattering efficiencies for homogeneous spherical particles of known size and complex RI are routinely computed at a specified wavelength by integrating the scattering intensity function over all scattering angles. Here however, we follow the procedure outlined by *Anderson et al.* [1996] and calculate Q_{sca} for both scattering and backscattering, appropriate to that directly measured by the nephelometer. This uses scattering angle dependent sensitivity functions (Ogren, personal communication, 2010) that reflect the optical characteristics of the nephelometer (TSI Model 3563), accounting for scattered light intensity losses (truncation) within the nephelometer at angles close to 0° and 180°. Correction of the nephelometer measured scattering is therefore unnecessary. The principal advantage of this method is that uncertainties associated with correcting the nephelometer measurements are entirely avoided. Scattering coefficients (σ_{sca}) are then computed in the usual way, as shown in equation (2), for particle diameters from 0.11 to 2.50 μm. As size- and time-dependent RI values are not available for supermicrometer particles, we substitute the corresponding values obtained for 1 μm particles. These are probably lower than the true values, which may be closer to 1.63 [*Eidhammer et al.*, 2008]. However, increasing RI for supermicrometer particles from those derived for 1 μm particles, to 1.65, only increases calculated overall scattering by ~2%.

4. Results and Discussion

4.1. Calculated Refractive Index

[22] Aerosol RI values and light scattering have been calculated for six representative days, two from each experimental campaign (23 July and 2 August 2005; 17 and 24 February 2006; and 3 August and 5 September 2006). These days were chosen to include both high and low scattering periods for each campaign. Unfortunately, instrument problems resulted in only a few days with comprehensive data sets in the first experimental period (summer 2005), with none exhibiting low scattering. Thus a combination of data from 2 and 3 August 2005 was used for the representative summer 2005 low-scattering day. Particulate chemical composition data were not available from the filters for 2 August 2005, while complete scattering data were unavailable for 3 August 2005. Consequently the analytical protocols using CE and mineral mass loading data from 3 August 2005, when aerosol mass loadings were low, were combined with the scattering, size distributions, and QAMS measurements on 2 August 2005. Very low scattering was observed on both 2 August 2005 and 24 February 2006, whereas the highest scattering was observed on 17 February 2006. On 5 September 2006, scattering in the morning was low, but subsequently increased due to wildfire smoke. Table 2 lists the QAMS CE for each of the six analysis days along with the daily averaged RI. The remaining columns of Table 2 are discussed below.

[23] Figure 4 displays variations of the calculated real RI on each day with time (Figure 4, top) and particle vacuum aerodynamic diameter (Figure 4, bottom). On 23 July 2005, the RI varies little throughout the day. Large real RIs are obtained for short periods on 2 August 2005 due to increases in the mass fraction of aerosol black carbon. On 17 February 2006, the real RI is ~1.50 early in the day, but then increases rapidly to 1.53. This change reflects increases of the relative mass concentrations of ammonium nitrate and ammonium sulfate. On both 3 August 2006 and 5 September 2006 (at EMO), the real RI displays little variability, being almost constant. The daily average RI values are given in Figure 4 (top). The six values show only small differences. *Guyon et al.* [2003] report similar small changes in RI, except at higher relative humidity (RH), when values tend to decrease. Our analyses are for periods when the RH was below 25%, thereby minimizing potential humidity effects.

[24] Variations of the average calculated real RI versus d_{va} from 0.04 to 1.0 μm, the upper size limit for size-dependent particle composition, are shown in Figure 4 (bottom) for each of the 6 days chosen for analysis. Expressing variations in RI as a function of d_{va} facilitates use of the QAMS mass loadings which vary with d_{va} but requires that the geometric diameters used for the BC size distribution are first converted to d_{va}, using the relationship given by *DeCarlo et al.* [2004]. The calculated RI values range from 1.46 to 1.60. In general, LAR particles with diameter less than 0.1 μm have low RI because with decreasing size, the mass fraction of

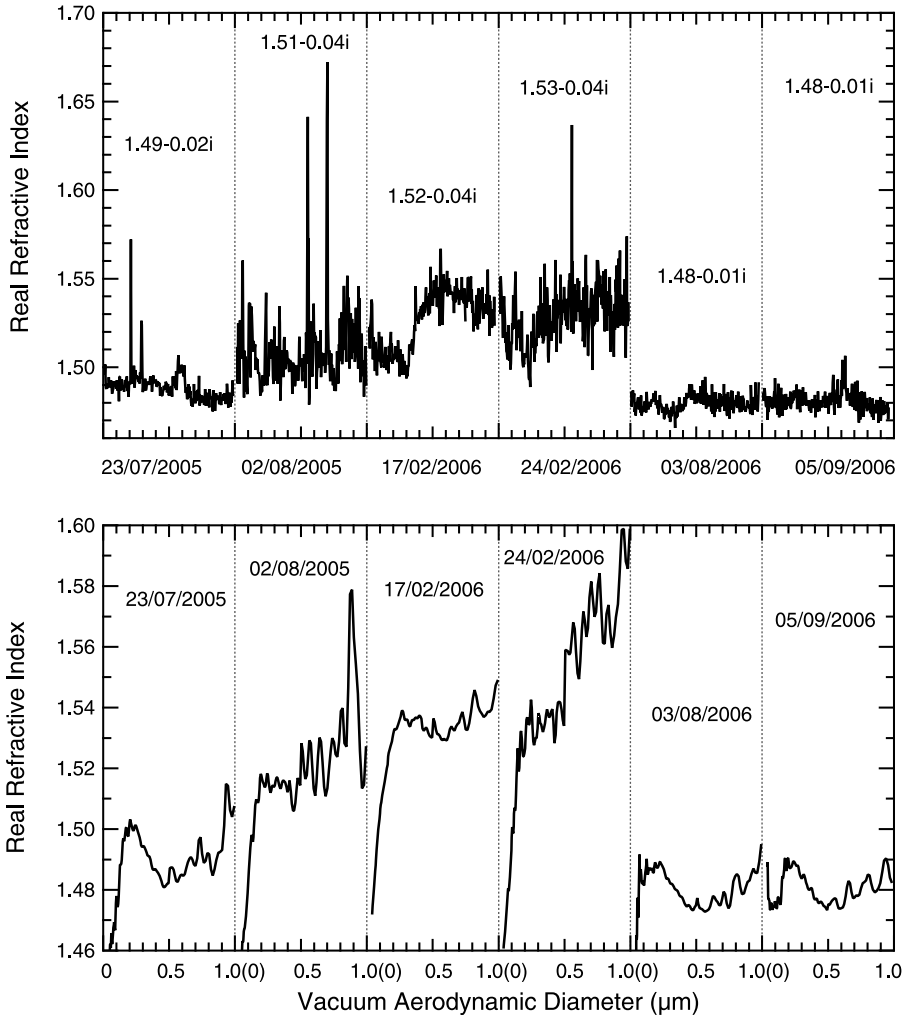

Figure 4. Variations of the estimated real refractive index at 550 nm wavelength with (top) time and (bottom) vacuum aerodynamic diameter. Each section separated by the dotted vertical lines represents 1 day or size range from 0 to 1.0 μm. Daily averaged refractive indices are also given in Figure 4 (top).

particulate organics increases, approaching 1.0 at the lower detection size limit of the QAMS. Thus for very small particles, the overall RI is essentially determined by that chosen for the organics. For larger particles from ~0.15 to ~0.5 μm, and for all those sampled at EMO, the mass fractions of other species, notably ammonium sulfate and ammonium nitrate, are nonnegligible, so that RI values are higher. The increase at larger particle diameters (>0.5 μm) reflects the contribution from mineral material. At EMO, where QAMS measurements show that organics dominate the aerosol composition and both BC and mineral mass fractions are low, <2.8% and <3.4%, respectively, RI values are generally lower than those in LAR and display less variability.

4.2. Refractive Index Uncertainties and Their Effect on Calculated Scattering

[25] Several factors contribute to uncertainty in the calculated RIs. Chief among these are uncertainties in aerosol species mass concentrations and individual RI values, especially for organics, and the method selected to distribute black carbon across the particle size spectrum. In addition, the unknown size distribution and less well-defined refractive index of mineral material, whose chemical identity is not well characterized, augment these uncertainties. However, the impact of these uncertainties is lessened by low BC and mineral mass loadings.

[26] To assess the sensitivity of calculated scattering and backscattering values on RI, calculations of scattering at a wavelength of 550 nm using a typical single daily averaged PCASP size distribution (that can be fitted by the power law function: N (cm$^{-3}\mu$m^{-1}) = 1.55 $D^{-4.34}$, where D = particle diameter (μm)) were carried out, in which the average real (but not the imaginary) part of the complex RI is varied. The ratios of calculated scattering and backscattering values, relative to those for a real RI of 1.59, are shown in Figure 5. RI = 1.59 is chosen as the fixed reference because it corresponds to that of PSL, normally used for PCASP calibration. Also shown in Figure 5 are plots of the ratios of both scattering and backscattering for particle size-corrected versus size-uncorrected PCASP size distributions as a function of real RI. This illustrates the well-known importance and magnitude of size corrections to PCASP measurements being used for scattering or backscattering

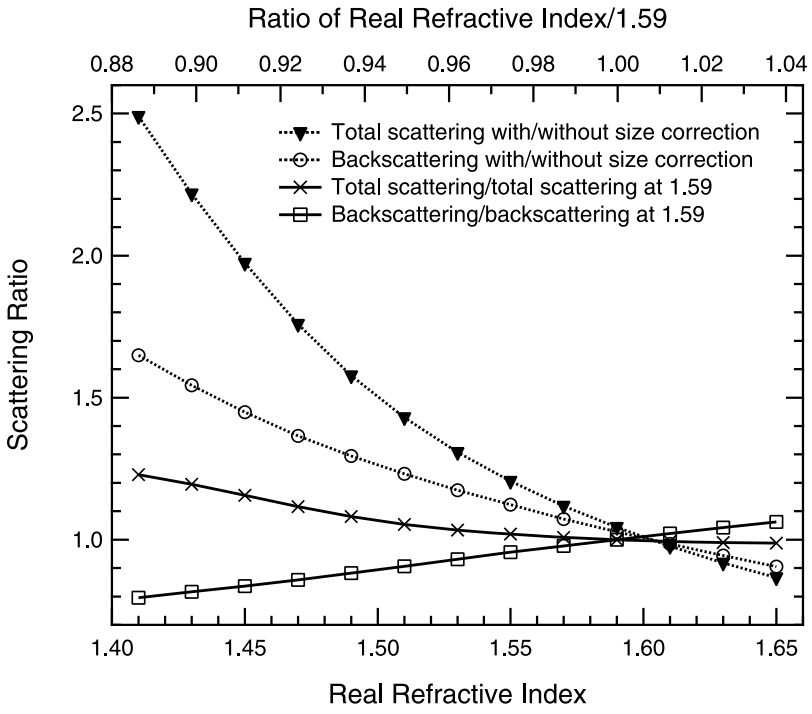

Figure 5. Ratios of calculated scattering (crosses) and backscattering (squares) for variable refractive indices compared to a refractive index of 1.59 at 550 nm wavelength (solid lines). Ratios of scattering (triangles) and backscattering (circles) for variable refractive index using PCASP sizes corrected for refractive index compared to sizes without correction (dashed lines).

calculations, when the RI of the ambient particles differs significantly from that of the PSL particles used for calibration [*Liu and Daum*, 2000; *Collins et al.*, 2000a]. Differences in scattering (backscattering) of 50 to >100% (25 to >50%) can occur if the PCASP is not corrected when the real RI is less than 1.50. For corrected PCASP sizes, the calculated ratio of scattering (backscattering) for any specified RI relative to that for RI = 1.59, increases (decreases) as real RI decreases. Within the RI range from 1.41 to 1.65, the relative change is <25% for scattering and <20% for backscattering. A much smaller dependence of calculated scattering on the value of the imaginary part of the RI, discussed subsequently in section 4.3, is also observed, leading to additional minor revisions of the PCASP size correction.

[27] Uncertainty arising from the unknown overall correction factor for BC mass loading (section 3.1) has but a minor effect on derived real RI values. Thus even for 17 February 2006, when BC relative mass loading was highest (7.9%), halving BC mass reduces RI by less than 1.0%. Similar reductions in BC on case study days when measured BC was lower result in smaller percentage changes in RI.

[28] Of somewhat greater importance is the assumed form of the BC size distribution. This has no effect on scattering and extinction calculated using non-size-dependent average and time-dependent RIs, but it can affect scattering calculated from the size-dependent RI. As outlined in section 3.1, BC was assumed to conform to a lognormal size distribution, with median size and width parameters equivalent to the SMPS volume size distribution. Choosing other median and width values allows the sensitivity of calculated scattering to the selected BC size distribution to be assessed. For a wavelength of 550 nm, either allowing the median diameter to vary over the range 0.15–0.4 μm or doubling the distribution width leads to changes in calculated scattering of less than 5% compared to that for a distribution centered on 0.25 μm. Thus, variations of the median size and width have only a slight influence on calculated scattering, which was expected since BC is but a small fraction of the total mass concentration, varying from a minimum of 2.1% at EMO on 3 August 2006 to a maximum of 7.9% at LAR on 17 February 2006.

[29] BC does, however, dominate the light absorbing characteristics of the aerosol, because contributions from other absorbing species, such as iron oxides, are negligibly small. Thus, uncertainties in both BC mass loading and size distribution affect the magnitude and size dependence of the imaginary part of the RI, with consequent significant effects on calculated absorption and single-scatter albedo. Varying the BC median diameter and size distribution width as before leads to changes in the calculated absorption coefficient of up to 42%. Thus, while the chosen BC size distribution affects calculated scattering minimally, calculated absorption as a function of particle size can be affected significantly.

[30] Average RIs for the particles and derived scattering are similarly insensitive to both the size distribution of the mineral material and its RI. The mass fraction of this material in the submicrometer size range is generally small, and its RI is only slightly larger than those of other particulate constituents (except for BC) [*Eidhammer et al.*, 2008]. Thus even for the extreme case of 24 February 2006 when the mineral mass fraction is at a maximum (16.9%), the calculated value of the average real RI is only increased

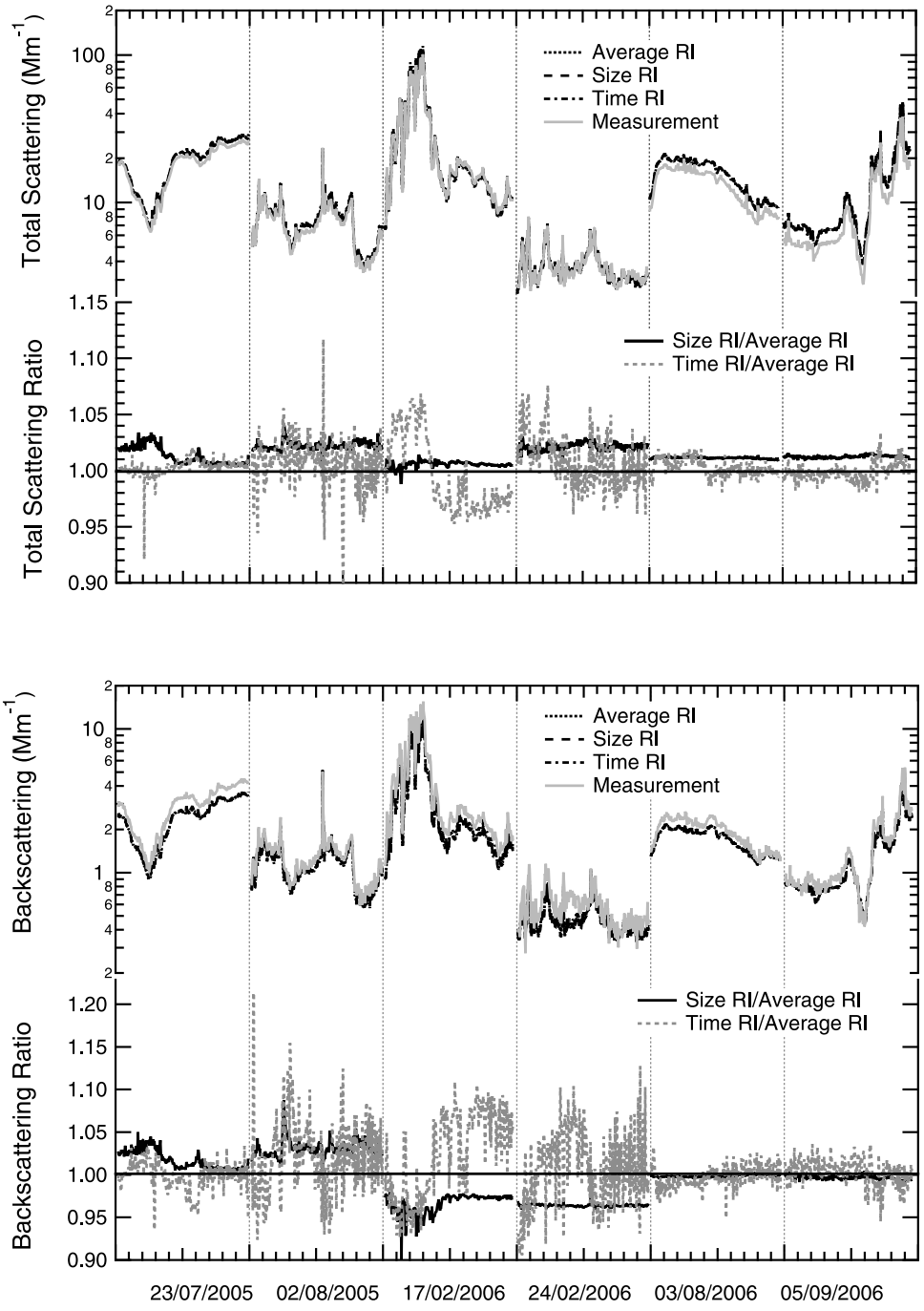

Figure 6. Measured and calculated scattering and backscattering at 550 nm from average, size-dependent, and time-dependent refractive indices, with 5 min time resolution. The impact of using size- or time-dependent RI versus average RI to calculate scattering/backscattering is shown as ratios of these quantities at the bottom of each frame. Dotted vertical lines delineate each analyzed 24 h period.

from 1.51 to 1.53 when mineral material is included in the particle composition.

4.3. Comparison of Calculated and Measured Scattering

[31] Scattering and backscattering coefficients appropriate to the nephelometer measurements (as described in section 3.5) were calculated using 5 min averages of the PCASP size distributions and time-dependent, size-dependent, and average RIs. The comparisons at 550 nm are shown in Figure 6. Scattering and backscattering, calculated from both time-dependent and size-dependent RI, are compared to that computed from average RI using ratios of these quantities, plotted in the lower part of each frame in Figure 6. The ratios for calculated total scattering from the time-dependent versus the average RI values show relatively high frequency variation, whereas those for size dependent versus average RIs display less variability, especially during summer 2006

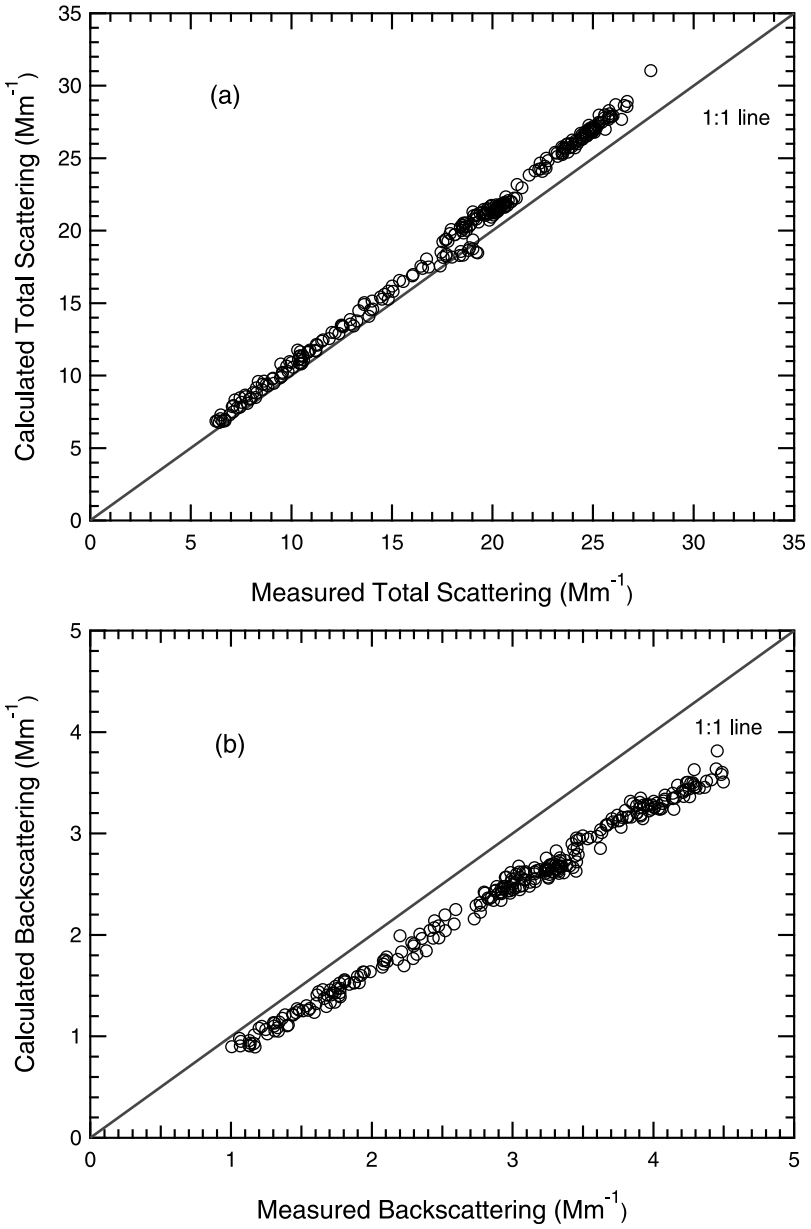

Figure 7. Comparison of the measured and calculated scattering coefficients using the average refractive index at 550 nm wavelength for 23 July 2005, (a) scattering and (b) backscattering, using corrected PCASP bin sizes.

at EMO. The ratios occasionally deviate from unity by more than 10% for short time intervals, but generally fall in the range 0.95–1.05. These results suggest that time-dependent aerosol scattering can be adequately calculated using 24 h average RI values and time-dependent size distribution measurements. Similar conclusions apply to backscattering, as shown in Figure 6 (bottom).

[32] Although calculated scattering time series using each of the RI values are similar, differences between calculated and measured scattering are readily discerned. A direct comparison of measured and calculated scattering at 550 nm on 23 July 2005, using the average RI, is shown in Figure 7, for corrected PCASP size distributions. The calculated scattering and backscattering are both linearly related to the corresponding measurements; however, calculated scattering slightly overestimates the measured values, while calculated backscattering underestimates the measurements. Linear regression slopes for the scattering and backscattering plots, forced through the plot origin, are 1.07 and 0.82 at 550 nm. Similar plots (not shown) can be constructed for other days, at each of the three wavelengths at which scattering and backscattering were measured. Table 2 summarizes the linear regression slopes for these plots for each day. The agreement between calculated and measured scattering and backscattering varies with wavelength. At 450 nm calculated scattering ranges from an underestimation of 6% to an overestimation of 17%, but generally overestimates measured scattering. This overestimation increases to 10%–39% at 700 nm. Calculated backscattering

underestimates the measured backscattering by 16%–29% at 450 nm, decreasing to 6%–19% at 700 nm.

[33] Measured scattering and backscattering are best compared with calculated values using RI values appropriate for each wavelength. Scattering and backscattering were therefore recalculated using particle RI values based on wavelength-dependent RI values for ammonium nitrate [*Merwin*, 1930], ammonium sulfate [*Toon et al.*, 1976], organic carbon [*Trentmann et al.*, 2002], and black carbon [*Kahnert*, 2010]. The wavelength-dependent RIs for the ammonium salts are both well characterized. The effect of uncertainties in the BC wavelength-dependent RI is minimized because the mass fraction of BC is low (2.1%–7.9%). These refinements change the agreement between the calculations and the measurements by less than 3% for all 6 days.

[34] Numerous factors influence the extent of agreement between the calculated and measured scattering. Aside from uncertainties in the measurements [*Anderson et al.*, 1996; *Anderson and Ogren*, 1998], these factors are principally associated with the accuracy, completeness, and resolution of the size distributions and RI values, the assumptions inherent in the Mie calculations, including those associated with the physical properties of the particle ensemble, and the corrections to account for instrument nonidealities. All of these factors affect the present results, to a greater or lesser degree. Addressing each one adequately is problematic and not always informative. Our calculation corrects for instrument nonidealities, but it assumes that the particles are spherical and internally mixed. In addition, error is introduced by using (corrected) size distributions based on PCASP measurements that divide the distribution into 30 size ranges of finite "bin width" and by ignoring scattering contributions from particles of diameter <0.1 μm. Particles <0.1 μm contribute <2% toward total scattering; however, their effect on backscatter may be somewhat more significant, an issue that merits further study.

[35] Within this mix of uncertainties affecting the comparisons, the greatest uncertainty in calculated scattering almost certainly arises from the poorly characterized value of organic species RI as a function of wavelength, especially as these species play a significant role in determining aerosol RI because of their large average mass fraction (40%–70%). To illustrate their importance we compare calculated and measured scattering for a range of RI values for organic species, with the results shown in Figure 8. As the real RI of the organics increases from the assumed value of 1.46, scattering decreases while backscattering (not shown) increases. The changes are most significant for 550 and 700 nm, with 450 nm showing only a slight dependence between 1.45 and 1.50. At 550 and 700 nm, the changes lead, on 4 of the 6 days, to values of organic species RI which give regression slopes of 1.0 when calculated and measured scattering are compared. The same adjustments to RI yield parallel improvements to the agreement of calculated and measured backscattering (not shown).

[36] While recognizing that the uncertainty in scattering measurements at 450, 550, and 700 nm are ±10% [*Anderson et al.*, 1996], optimal agreement between calculated and measured scattering is achieved at all three wavelengths if the real RI of organic material is either in the range 1.42–1.67 (wavelength-independent) or 1.45 ± 0.02, 1.51 ± 0.04, and 1.62 ± 0.05 at wavelengths of 450, 550, and 700 nm (wavelength-dependent). These refractive indices are somewhat larger than those often suggested [*Stelson*, 1990; *Trentmann et al.*, 2002] but are not without precedent. *Collins et al.* [2000a] followed the original suggestion of *Sloane* [1984] and used 1.55 at 550 nm for organic material when calculating RI from particle compositions. *Hand and Kreidenweis* [2002] showed that, at Big Bend National Park, a RI of 1.55 for the organics leads to a particle RI that is commensurate with that retrieved by comparing optical and mobility measured size distributions. *McMeeking et al.* [2005] refined this method, corroborating *Hand and Kreidenweis*' result. By combining the retrieved real part of the RI, with those of the imaginary part derived from particle composition, *McMeeking et al*. showed that for dry submicrometer particles sampled in Yosemite National Park, calculated and measured scattering were in reasonably good agreement. These studies along with the work here suggest that at least some kinds of aerosol organic material have high RIs, which is consistent with high RI values measured for some oxygenated organic species likely to be present in the aerosol. For example, at 532 nm, *Hoffer et al.* [2006] and *Dinar et al.* [2008] report values ≥1.56 for several HULIS (humic-like substances) samples. Mass spectral analyses of the organic material present in our sampled aerosol indicate that a significant fraction (0.4–0.7 in summer) has undergone oxidative aging and has a high organic mass to organic carbon mass ratio (2.6 ± 0.1), which could imply a high RI.

[37] Calculated scattering can also be affected by the imaginary part of the RI when the mass fractions of absorbing species are high. That is not the case here as mass fractions of the only significant absorbing species, BC, are generally low, particularly at EMO (2.1% and 2.8% for the two case study days). Consequently, even for the highest BC mass fraction (7.9%), measured at LAR on 17 February 2006, an uncertainty of 50% in the imaginary part of the RI leads to an uncertainty of only 2% in calculated total scattering at 550 nm and no more than 7% for backscattering. Uncertainties in BC mass loading also affect calculated scattering and backscattering via their modest influence on the real part of the RI (section 4.2). For a 50% reduction in BC on 17 February 2006, slopes of the correlation plots of calculated versus measured scattering at 550 nm (Figure 7) undergo a change of no more than 1%, while those for backscattering show a maximum 5% change. Lower BC mass fractions result in correspondingly lower scattering uncertainties.

[38] Better agreement is achieved for the first four case study days investigated than for the measurements on the last 2 days at EMO, where calculated scattering extinctions at 550 nm exceed those measured by ~10% on 3 August 2006 and ~17% on 5 September 2006, for a real RI of 1.51 for the organics. These differences, which are reduced slightly at higher RI values, are similar to those reported by others [e.g., *Collins et al.*, 2000a], and they are less than the expected minimum uncertainty, typically ~20%, for comparable optical closure studies [e.g., *Horvath*, 1998; *Quinn et al.*, 2004]. Differences in the composition of the aerosol at EMO compared to that at LAR cannot alone explain these discrepancies. Measured scattering is always less than that calculated for any reasonable RI value, as the plots for 3 August 2006 and 5 September 2006 in Figure 8 show. The

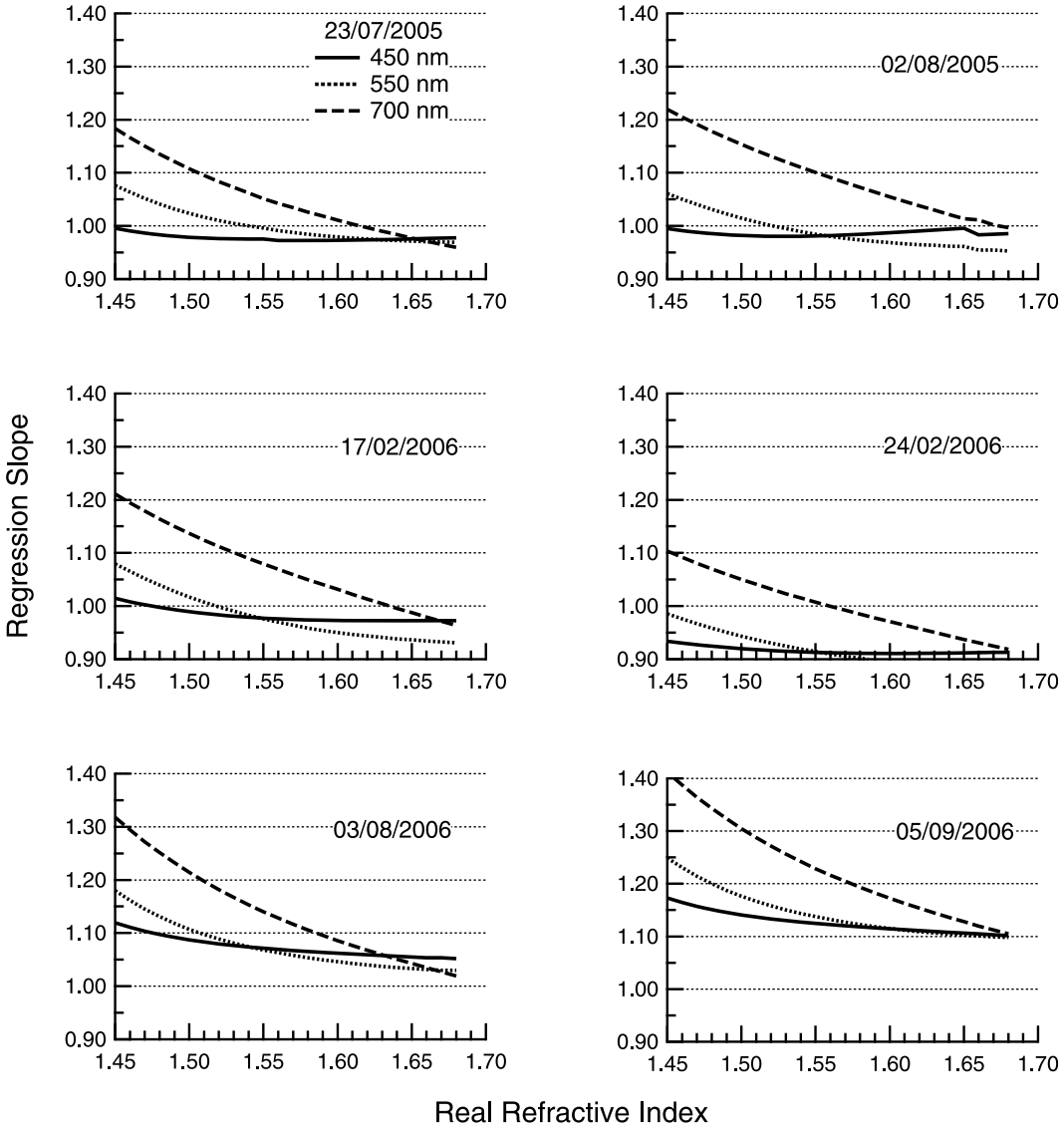

Figure 8. Ratio of calculated to measured scattering for variable real refractive index of organic material.

explanation must therefore lie with uncertainties in either measured scattering or measured particle size distributions. Defining particle size distributions with adequate precision is particularly relevant, as calculated scattering is sensitive to both the corrected diameters of the PCASP bins and to the number densities of particles in each bin. This factor alone could account for the observed small differences.

[39] In addition to scattering coefficients, Mie calculations yield estimates of aerosol absorption coefficients when the imaginary part of the RI is nonzero. Because BC is assumed to be the sole important contributor to light absorption, calculated absorptions mirror the temporal variations of BC mass concentration. Figure 9 shows measured BC mass concentrations and the calculated absorption coefficients for 23 July 2005 using time-dependent, size-dependent, and average RI values. Calculated absorption coefficients are usually less than 10 Mm^{-1}, with the three daily averages in good agreement. However, in contrast to comparisons of temporal variations in scattering coefficient, those for the absorption coefficients show that while coefficients calculated using the average and size-dependent RI vary minimally, those obtained with the time-dependent indices exhibit large short-term variations, in parallel with observed BC mass loading variations. This reflects changes in the imaginary RI that occur in parallel with the short term changes in BC mass concentration. In contrast, the real RI and scattering coefficients are affected minimally by changes in BC concentration, because they are largely determined by the other aerosol components that have greater mass fractions.

4.4. Single-Scatter Albedo

[40] Combining scattering and absorption coefficients enables estimates of the single-scatter albedo (SSA), the ratio of total scattering to total extinction, to be made. SSA has particular relevance when modeling aerosol radiative effects that influence climate forcing [*Haywood and Shine*, 1995]. Observed SSA values (SSA_{obs}) are readily obtained

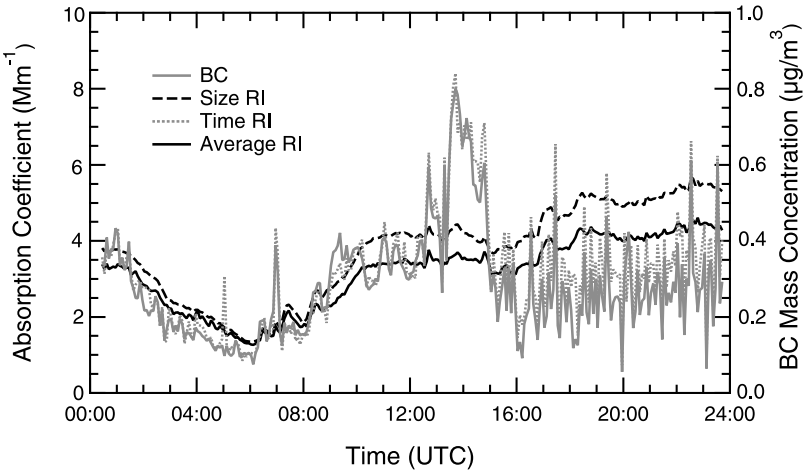

Figure 9. Calculated absorption coefficients at 550 nm from average, size-dependent, and time-dependent refractive indices using the corrected PCASP size distribution for 23 July 2005. Variation of black carbon mass concentration (right-hand axis) with time is also plotted. Data points are 5 min averages.

from the measured scattering and absorption. In this case, the scattering measured by the nephelometer must be corrected, using the method of *Anderson and Ogren* [1998], to obtain the true total scattering over all angles. In this method, Ångstrom exponents are first derived and then used to calculate scattering correction factors that correct for non-Lambertian and truncation nonidealities in the nephelometer. Multiplying measured scattering by the correction factor yields total scattering. Absorption is derived from the measured BC mass loadings. In common with many previously reported studies, we use a mass absorption coefficient of 10 m^2/g, a value appropriate for aged atmospheric BC containing particles. The validity of this value, which is ~30% larger than that recommended for freshly generated BC, has been discussed by *Bond and Bergstrom* [2006]. Calculated SSA values (SSA_{calc}) are determined directly from the total scattering and absorption coefficients computed by Mie calculations over all angles. We have evaluated SSA_{calc} at 550 nm wavelength using both the time-dependent and average RI values together with the corresponding corrected 5 min average PCASP size distributions and compared them to SSA_{obs} for each case study day. The comparisons are shown in Figure 10. Twenty-four hour averages and standard deviations of SSA_{obs} and SSA_{calc} are listed in Table 3. Uncertainties related to assumptions about the size distribution of BC do not enter these calculations since we do not use a size-dependent refractive index for these comparisons.

[41] SSA_{obs} displays irregular diurnal variability, primarily reflecting variations in BC mass loading. BC emissions are invariably dominated by combustion sources associated with human activities [*Bond et al.*, 2004], which might be anticipated to maximize during the daytime. BC surface concentrations vary considerably however, as illustrated for 23 July 2005 in Figure 9. The concentrations are strongly affected not only by the source strength of the BC, but also by continually varying meteorological factors such as ventilation and depth of the mixed layer. Consequently no distinct persistent diurnal variability pattern for SSA_{obs} can be established. At EMO in summer, SSA_{obs} values are high (~0.95) and vary little, underlining our conclusion based on the observed low scattering extinction that air at this site is minimally polluted and that it is frequently one of the cleanest midcontinental surface sampling locations in the United States. In LAR, SSA_{obs} occasionally falls to <0.5 for very short intervals when BC-rich plumes are intercepted, but, in general, values are in the range 0.7–0.9. Values tend to be slightly lower in winter than in summer, probably reflecting the impact of woodsmoke from domestic heating stoves being trapped in a shallow surface inversion layer. Time-dependent SSA_{obs} and SSA_{calc} with time-dependent RIs agree well, as do 24 h average SSA_{obs} and SSA_{calc} using average RIs, especially given the uncertainties associated with the BC mass absorption coefficient, the RIs for BC, minerals, and the organics, and the largely unknown mixing state and morphologies of the aerosol particles. Differences between SSA_{obs} and SSA_{calc} with the average RI are generally <3%, except on 2 August 2005 when the difference rose to near 5%.

[42] While there is good agreement between SSA_{obs} and SSA_{calc}, both parameters are derived in part using the BC mass loading, so their values are sensitive to uncertainties in BC, especially when the BC mass loading is high. Thus, on 17 February 2006, when BC was highest, SSA_{calc} at 550 nm increases by 10.9% for a 50% reduction in BC, while SSA_{obs} increases by 9.9%. For case study days where measured BC is lower, such as 5 September 2006 when (uncorrected) BC contributes only 2.8% to the total aerosol mass, a similar 50% reduction in BC increases SSA_{calc} at 550 nm by 3.0% and SSA_{obs} by 2.7%. To the extent that BC mass loadings are uncertain, absolute values of SSA will be uncertain and the range of SSA cannot be definitively assessed. This reemphasizes the importance of determining BC mass loadings with high accuracy, especially when BC contributes significantly to the total aerosol mass.

5. Summary and Conclusions

[43] Surface aerosols were sampled continuously for three 2 week periods in Laramie, Wyoming, in summer 2005 and

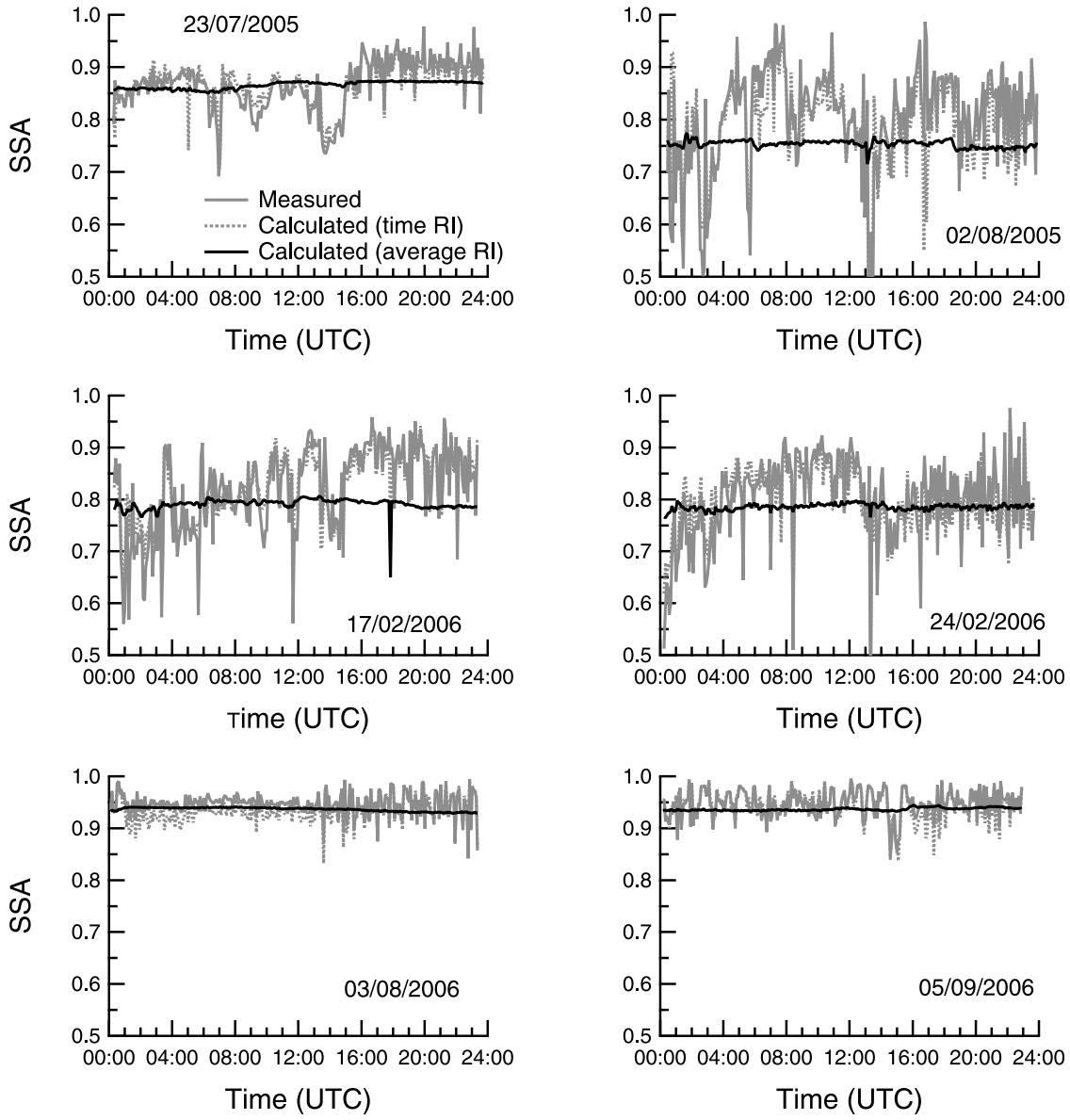

Figure 10. Diurnal variations of single-scatter albedo (SSA) derived from observed scattering and black carbon mass loading and calculated SSA using time-dependent and averaged refractive indices at 550 nm wavelength.

winter 2006, and at Elk Mountain Observatory, on a nearby remote mountain top, in summer 2006. Aerosol size distributions were measured with a PCASP, SMPS, and UHSAS, aerosol absorption with an aethalometer, composition with an Aerodyne quadrupole aerosol mass spectrometer and filters, and light scattering with a nephelometer. The aerosol composition measurements are used to estimate three types of aerosol refractive index: an average, a size-dependent, and a time-dependent index. The daily average real RI, computed from the mass concentration measurements in the three periods, varies minimally, with the least variation on Elk Mountain. The ambient aerosol RI values are used to correct the PCASP sizes. Averages of the measured scattering at 550 nm are 12.8 ± 6.5 Mm^{-1} in Laramie in summer, 7.7 ± 8.3 Mm^{-1} in Laramie in winter, and 11.2 ± 8.7 Mm^{-1}, on Elk Mountain in summer. Observed time-dependent aerosol scattering is compared with that calculated from the corrected measured PCASP size distributions and the average, size-dependent, and time-dependent RI values. Scattering calculated from these three RIs differs on

Table 3. Observed and Calculated Single-Scatter Albedo at 550 nm[a]

Date	SSA_{obs} (24 h Average)	SSA_{calc} (24 h Average)
23 July 2005	0.865 ± 0.047	0.866 ± 0.007
2 August 2005	0.800 ± 0.102	0.753 ± 0.007
17 February 2006	0.820 ± 0.083	0.791 ± 0.011
24 February 2006	0.799 ± 0.080	0.785 ± 0.006
3 August 2006	0.946 ± 0.022	0.936 ± 0.004
5 September 2006	0.947 ± 0.026	0.937 ± 0.003

[a]Twenty-four hour averages and standard deviations are listed. SSA, single-scatter albedo.

average by less than 5%. For short time intervals differences occasionally exceed 10%. For the six case study days, the calculated scattering (backscattering) at 550 nm ranges from 2% smaller to 23% larger (11%–22% smaller) than that measured. These differences decrease at 450 nm and increase at 700 nm and also increase (decrease) significantly if the optical size distribution measurements are not corrected for index of refraction. The calculated scattering could be matched with measurement values at all three wavelengths on four of the 6 days investigated, if the real RI values of organic carbon, which are not well known, are adjusted to be 1.45 ± 0.02, 1.51 ± 0.04, and 1.62 ± 0.05 at wavelengths of 450, 550, and 700 nm, respectively. For the other 2 days, differences between calculated and measured scattering cannot be correspondingly reduced, but they are still less than those expected from measurement uncertainties. Single-scatter albedos, derived from measured scattering and mass loadings of black carbon, the principal absorbing species, are in the range 0.79–0.87 in Laramie and ~0.95 on Elk Mountain, where pristine conditions frequently prevail. Calculated single-scatter albedo values determined by Mie calculations using both time-dependent and averaged refractive indices are within 5% of those derived directly from the observations. This good agreement would be maintained even if the absolute values of single-scatter albedo are in error due to uncertainties in black carbon mass loading.

[44] **Acknowledgments.** This work was supported by the National Science Foundation under grant ATM-0441836 and the W. M. Keck Foundation. The significant effort of the department's technical staff in preparing instrumentation for the Laramie measurements and in deploying instrumentation to EMO is gratefully acknowledged.

References

Anderson, T. L., and J. A. Ogren (1998), Determining aerosol radiative properties using the TSI 3563 integrating nephelometer, *Aerosol Sci. Technol.*, *29*, 57–69.

Anderson, T. L., et al. (1996), Performance of a high-sensitivity, three-wavelength, total scatter/backscatter nephelometer, *J. Atmos. Oceanic Technol.*, *13*, 967–986.

Anderson, T. L., D. S. Covert, J. D. Wheeler, J. M. Harris, K. D. Perry, B. E. Trost, D. J. Jaffe, and J. A. Ogren (1999), Aerosol backscatter fraction and single-scatter albedo: Measured values and uncertainties at a coastal station in the Pacific Northwest, *J. Geophys. Res.*, *104*(D21), 26,793–26,807, doi:10.1029/1999JD900172.

Arnott, W. P., K. Hamasha, H. Moosmüller, P. J. Sheridan, and J. A. Ogren (2005), Toward aerosol light-absorption measurements with a 7-wavelength aethalometer: Evaluation with a photoacoustic instrument and 3-wavelength nephelometer, *Aerosol Sci. Technol.*, *39*, 17–29, doi:10.1080/027868290901972.

Barnaba, F., A. M. Tafuro, F. De Tomaci, and M. R. Perrone (2007), Observed and simulated vertically resolved optical properties of continental aerosols over southeastern Italy: A closure study, *J. Geophys. Res.*, *112*, D10203, doi:10.1029/2006JD007926.

Bohren, C. F., and D. R Huffman (1983), *Absorption and Scattering of Light by Small Particles*, Wiley, New York.

Bond, T. C., and R. W. Bergstrom (2006), Light absorption by carbonaceous particles: An investigative review, *Aerosol Sci. Technol.*, *40*, 27–67.

Bond, T. C., D. G. Streets, K. F. Yarber, S. M. Nelson, J.-H. Woo, and Z. Klimont (2004), A technology based global inventory of black and organic carbon emissions from combustion, *J. Geophys. Res.*, *109*, D14203, doi:10.1029/2003JD003697.

Cai, Y., D. C. Montague, W. Mooiweer-Bryan, and T. Deshler (2008), Performance characteristics of the ultrahigh sensitivity aerosol spectrometer for particles between 55 and 800 nm: Laboratory and field studies, *J. Aerosol Sci.*, *39*, 759–769.

Canagaratna, M. R., et al. (2007), Chemical and microphysical characterization of ambient aerosols with the Aerodyne aerosol mass spectrometer, *Mass Spectrom. Rev.*, *26*(2), 185–222.

Cheng, Y. F., et al. (2008), Aerosol optical properties and related chemical apportionment at Xinken in Pearl River Delta of China, *Atmos. Environ.*, *42*, 6351–6372.

Chow, J. C., and J. G. Watson (1999), Ion chromatography, in *Elemental Analysis of Airborne Particles*, edited by S. Landsberger and M. Creatchman, pp. 97–137, Gordon and Breach, Newark, N. J.

Clarke, A. D., et al. (2004), Size distributions and mixtures of dust and black carbon aerosol in Asian outflow: Physiochemistry and optical properties, *J. Geophys. Res.*, *109*, D15S09, doi:10.1029/2003JD004378.

Collaud Coen, M., et al. (2010), Minimizing light absorption measurement artifacts of the Aethalometer: Evaluation of five correction algorithms, *Atmos. Meas. Technol.*, *3*, 457–474.

Collins, D. R., et al. (2000a), In situ aerosol size distributions and clear-column radiative closure during ACE-2, *Tellus, Ser B*, *52*, 498–525.

Collins, D. R., H. H. Jonsson, H. Liao, R. C. Flagan, J. H. Seinfeld, K. J. Noone, and S. V. Hering (2000b), Airborne analysis of the Los Angeles aerosol, *Atmos. Environ.*, *34*, 4155–4173.

Cook, J., E. J. Highwood, H. Coe, P. Formenti, J. M. Haywood, and J. Crosier (2007), A comparison of aerosol optical and chemical properties over the Adriatic and Black seas during summer 2004: Two case studies from ADRIEX, *Q. J. R. Meteorol. Soc.*, *133*(S1), 33–35.

Cross, E. S., J. G. Slowik, P. Davidovits, J. D. Allan, D. R. Worsnop, J. T. Jayne, D. K. Lewis, M. Canagaratna, and T. B. Onsach (2007), Laboratory and ambient particle density determinations using light scattering in conjunction with aerosol mass spectrometry, *Aerosol Sci. Technol.*, *41*, 343–359.

DeCarlo, P. F., J. G. Slowik, D. R. Worsnop, P. Davidovits, and J. L. Jimenez (2004), Particle morphology and density characterization by combined mobility and aerodynamic diameter measurements: Part 1. Theory, *Aerosol Sci. Technol.*, *38*, 1185–1205.

de Reuss, M., P. Formenti, J. Ström, R. Krejci, D. Müller, M. O. Andreae, and J. Lelieveld (2002), Airborne observations of dry particle absorption and scattering properties over the northern Indian Ocean, *J. Geophys. Res.*, *107*(D22), 8002, doi:10.1029/2002JD002304.

Delene, D. J., and T. Deshler (2000), Calibration of a photometric cloud condensation nucleus counter designed for deployment on a balloon package, *J. Atmos. Oceanic Technol.*, *17*, 459–467.

Delene, D. J., and J. A. Ogren (2002), Variability of aerosol optical properties at four North American surface monitoring sites, *J. Atmos. Sci.*, *59*, 1135–1150.

Deshler, T., B. Nardi, A. Adriani, F. Cairo, G. Hansen, F. Fierli, A. Hauchercorne, and L. Pulvirenti (2000), Determining the index of refraction of polar stratospheric clouds above Andoya (69°N) by combining size-resolved concentration and optical scattering measurements, *J. Geophys. Res.*, *105*(D3), 3943–3953, doi:10.1029/1999JD900469.

Dinar, E., A. Abo Riqziq, C. Spindler, C. Erlick, G. Kiss, and Y. Rudich (2008), The complex refractive index of atmospheric and model humic-like substances (HULIS) retrieved by a cavity ring down aerosol spectrometer (CRD-AS), *Faraday Disc.*, *137*, 279–295.

Ebert, M., S. Weinbruch, P. Hoffmann, and H. M. Ortner (2004), The chemical composition and complex refractive index of rural and urban influenced aerosols determined by individual particle analysis, *Atmos. Environ.*, *38*, 6531–6545.

Eidhammer, T., D. C. Montague, and T. Deshler (2008), Determination of index of refraction and size of supermicrometer particles from light scattering measurements at two angles, *J. Geophys. Res.*, *113*, D16206, doi:10.1029/2007JD009607.

Gebhart, K. A., S. Copland, and W. C. Malm (2001), Diurnal and seasonal patterns in light scattering, extinction, and relative humidity, *Atmos. Environ.*, *35*, 5177–5191.

Guyon, P., O. Boucher, B. Graham, J. Beck, O. L. Mayol-Bracero, G. C. Roberts, W. Maenhaut, P. Artaxo, and M. O. Andreae (2003), Refractive index of aerosol particles over the Amazon tropical forest during LBA-EUSTACH 1999, *J. Aerosol Sci.*, *34*(7), 883–907.

Han, Z. G., D. C. Montague, and J. R. Snider (2003), Airborne measurements of aerosol extinction in the lower and middle troposphere over Wyoming, USA, *Atmos. Environ.*, *37*, 789–802.

Hand, J. L., and S. M. Kreidenweis (2002), A new method for retrieving particle refractive index and effective density from aerosol size distribution data, *Aerosol Sci. Technol.*, *36*(10), 1012–1026.

Hansen, A. D. A., H. Rosen, and T. Novakov (1984), The aethalometer—An instrument for the real-time measurement of optical absorption by aerosol particles, *Sci. Total Environ.*, *36*, 191–196.

Hasan, H., and T. G. Dzubay (1983), Apportioning light extinction coefficients to chemical species in atmospheric aerosol, *Atmos. Environ.*, *17*, 1573–1581.

Haywood, J. M., and K. P. Shine (1995), The effect of anthropogenic sulfate and soot aerosol on the clear-sky planetary radiation budget, *Geophys. Res. Lett.*, *22*(5), 603–606, doi:10.1029/95GL00075.

Hitzenberger, R., and S. Tohno (2001), Comparison of black carbon (BC) aerosols in two urban areas – Concentrations and size distributions, *Atmos. Environ.*, *35*, 2153–2167.

Hoffer, A., A. Gelencsér, P. Guyon, G. Kiss, O. Schmid, G. P. Frank, P. Artaxo, and M. O. Andreae (2006), Optical properties of humic-like substances (HULIS) in biomass-burning aerosols, *Atmos. Chem. Phys.*, *6*, 3563–3570.

Horvath, H. (1998), Influence of atmospheric aerosols upon the global radiation balance, in *Atmospheric Particles*, edited by R. M. Harrison and R. Van Grieken, p. 543, Wiley, New York.

Huffman, J. A., J. T. Jayne, F. Drewnick, A. C. Aiken, T. Onasch, D. R. Worsnop, and J. L. Jimenez (2005), Design, modeling, optimization, and experimental tests of a particle beam width probe for the Aerodyne Aerosol Mass Spectrometer, *Aerosol Sci. Technol.*, *39*, 1143–1163.

Intergovernmental Panel on Climate Change (IPCC) (2007), *Scientific Basis, Fourth Assessment of the Intergovernmental Panel on Climate Change*, Cambridge Univ. Press, New York.

Jayne, J. T., D. C. Leard, X. Zhang, P. Davidovits, K. A. Smith, C. E. Kolb, and D. R. Worsnop (2000), Development of an aerosol mass spectrometer for size and composition analysis of submicron particles, *Aerosol Sci. Technol.*, *33*, 49–70.

Jimenez, J. L., et al. (2003), Ambient aerosol sampling using the Aerodyne Aerosol Mass Spectrometer, *J. Geophys. Res.*, *108*(D7), 8425, doi:10.1029/2001JD001213.

Kahnert, M. (2010), Modelling the optical and radiative properties of freshly emitted light absorbing carbon within an atmospheric chemical transport model, *Atmos. Chem. Phys.*, *10*, 1403–1416.

Kim, Y. J., and J. F. Boatman (1990a), The effects that the optical properties of particles have on atmospheric aerosol measurements with optical particle spectrometers, *J. Aerosol Sci.*, *21*, suppl. 1, S551–S554.

Kim, Y. J., and J. F. Boatman (1990b), Size calibration corrections for the active scattering aerosol spectrometer probe (ASASP-100X), *Aerosol Sci. Technol.*, *12*, 665–672.

Liu, P. S. K., R. Deng, K. A. Smith, L. R. Williams, J. T. Jayne, M. R. Canagaratna, K. Moore, T. B. Onasch, D. R. Worsnop, and T. Deshler (2007), Transmission efficiency of an aerodynamic focusing lens system: Comparison of model calculations and laboratory measurements for the Aerodyne aerosol mass spectrometer, *Aerosol Sci. Technol.*, *41*, 721–733.

Liu, Y. G., and P. H. Daum (2000), The effect of refractive index on size distributions and light scattering coefficients derived from optical particle counters, *J. Aerosol Sci.*, *31*(8), 945–957.

Lowenthal, D. H., J. G. Watson, and P. Saxena (2000), Contributions to light extinction during project MOHAVE, *Atmos. Environ.*, *34*, 2351–2359.

Lyamani, H., F. J. Olmo, and L. Alados-Arboledas (2008), Light scattering and absorption properties of aerosol particles in the urban environment of Granada, Spain, *Atmos. Environ.*, *42*, 2630–2642.

Malm, W. C., D. E. Day, C. Carrico, S. M. Kreidenweis, J. L. Collett Jr., G. McKeeking, T. Lee, J. Carillo, and B. Schichtel (2005), Intercomparison and closure calculations using measurements of aerosol species and optical properties during the Yosemite aerosol characterization study, *J. Geophys. Res.*, *110*, D14302, doi:10.1029/2004JD005494.

Massoli, P., T. S. Bates, P. K. Quinn, D. A. Lack, T. Baynard, B. M. Lerner, S. C. Tucker, J. Brioude, A. Stohl, and E. J. Williams (2009), Aerosol optical and hygroscopic properties during TexAQS-GoMACCS 2006 and their impact on aerosol direct radiative forcing, *J. Geophys. Res.*, *114*, D00F07, doi:10.1029/2008JD011604.

Matthew, B. M., A. M. Middlebrook, and T. B. Onasch (2008), Collection efficiencies in an Aerodyne aerosol mass spectrometer as a function of particle phase for laboratory generated aerosols, *Aerosol Sci. Technol.*, *42*(11), 884–898.

McMeeking, G. R., S. M. Kreidenweis, C. M. Carrico, J. L. Collett, D. E. Day, and W. C. Malm (2005), Observations of smoke-influenced aerosol during the Yosemite aerosol characterization study: 2. Aerosol scattering and absorbing properties, *J. Geophys. Res.*, *110*, D18209, doi:10.1029/2004JD005624.

Merwin, H. E. (1930), *International Critical Tables of Numerical Data: Physics, Chemistry and Technology*, vol. 7, pp. 16–33, McGraw-Hill, New York.

Ouimette, J. R., and R. C. Flagan (1982), The extinction coefficient of multicomponent aerosols, *Atmos. Environ.*, *16*, 2405–2419.

Pesava, P., H. Horvath, and M. Kasahara (2001), A local optical closure experiment in Vienna, *J. Aerosol Sci.*, *32*, 1249–1267.

Philippin, S., C. Neusüß, A. Wiedensohler, J. Heintzenberg, C. M. Carrico, and M. J. Rood (1998), Optical properties of anthropogenically influenced aerosols in a marine atmosphere: An optical closure experiment, *J. Aerosol Sci.*, *29*, suppl. 2, S1151–S1152.

Quinn, P. K., and D. J. Coffman (1998), Local closure during the First Aerosol Characterization Experiment (ACE 1): Aerosol mass concentration and scattering and backscattering coefficients, *J. Geophys. Res.*, *103*(D13), 16,575–16,596, doi:10.1029/97JD03757.

Quinn, P. K., T. L. Anderson, T. S. Bates, R. Dlugi, J. Heintzenberg, W. von Hoyningen-Huene, M. Kulmala, P. B. Russell, and E. Swietlicki (1996), Closure in tropospheric aerosol-climate research: A review and future needs for addressing aerosol direct shortwave radiative forcing, *Beitr. Phys. Atmos.*, *69*, 547–577.

Quinn, P. K., et al. (2004), Aerosol optical properties measured on board the Ronald H. Brown during ACE-Asia as a function of aerosol chemical composition and source region, *J. Geophys. Res.*, *109*, D19S01, doi:10.1029/2003JD004010.

Redemann, J., et al. (2000), Retrieving the vertical structure of the effective aerosol complex index of refraction from a combination of aerosol in situ and remote sensing measurements during TARFOX, *J. Geophys. Res.*, *105*(D8), 9949–9970, doi:10.1029/1999JD901044.

Ross, J. L., P. V. Hobbs, and B. Holben (1998), Radiative characteristics of regional hazes dominated by smoke from biomass burning in Brazil: Closure tests and direct radiative forcing, *J. Geophys. Res.*, *103*(D24), 31,925–31,941, doi:10.1029/97JD03677.

Schkolnik, G., D. Chand, A. Hoffer, M. O. Andreae, C. Erlick, E. Swietlicki, and Y. Rudich (2007), Constraining the density and complex refractive index of elemental and organic carbon in biomass burning aerosol using optical and chemical measurements, *Atmos. Environ.*, *41*(5), 1107–1118.

Schmid, O., P. Artaxo, W. P. Arnott, D. Chand, L. V. Gatti, G. P. Frank, A. Hoffer, M. Schnaiter, and M. O. Andreae (2006), Spectral light absorption by ambient aerosols influenced by biomass burning in the Amazon Basin: I. Comparison and field calibration of absorption measurement techniques, *Atmos. Chem. Phys.*, *6*, 3443–3462.

Schwartz, J. P., et al. (2008a), Measurement of the mixing state, mass, and optical size of individual black carbon particles in urban and biomass burning emissions. *Geophys. Res. Lett.*, *35*, L13810, doi:10.1029/2008GL033968.

Schwartz, J. P., et al. (2008b), Coatings and their enhancement of black carbon light absorption in the tropical atmosphere, *J. Geophys. Res.*, *113*, D03203, doi:10.1029/2007JD009042.

Sloane, C. S. (1984), Optical properties of aerosols of mixed composition, *Atmos. Environ.*, *18*, 871–878.

Snider, J. R., and J.-L. Brenguier (2000), Cloud condensation nuclei and cloud droplet measurements during ACE-2, *Tellus, Ser B*, *52*, 828–842.

Stelson, A. W. (1990), Urban aerosol refractive index prediction by partial molar refraction approach, *Environ. Sci. Technol.*, *24*, 1676–1679.

Stratmann, F., et al. (2010), An overview of the LACIS experiment in November (LexNo) campaign, *J. Geophys. Res.*, *115*, D11203, doi:10.1029/2009JD012628.

Swartzendruber, P. C., D. Chand, D. A. Jaffe, J. Smith, D. Reidmiller, L. Gratz, J. Keeler, S. Strode, L. Jaeglé, and R. Talbot (2008), Vertical distribution of mercury, CO, ozone, and aerosol scattering coefficient in the Pacific Northwest during the spring 2006 INTEX-B campaign, *J. Geophys. Res.*, *113*, D10305, doi:10.1029/2007JD009579.

Takegawa, N., Y. Miyazaki, Y. Kondo, Y. Komazaki, T. Miyakawa, J. Jimenez, J. T. Jayne, D. R. Worsnop, J. Allen, and R. J. Weber (2005), Characterization of an Aerodyne aerosol mass spectrometer (AMS): Intercomparison with other aerosol instruments, *Aerosol Sci. Technol.*, *39*, 760–770.

Toon, O. B., J. B. Pollack, and B. N. Khare (1976), The optical constants of several atmospheric aerosol species: Ammonium sulfate, aluminum oxide, and sodium chloride, *J. Geophys. Res.*, *81*(33), 5733–5748, doi:10.1029/JC081i033p05733.

Trentmann, T., M. O. Andreae, H. F. Grat, P. V. Hobbs, R. D. Ottmar, and T. Trautmann (2002), Simulation of a biomass-burning plume: Comparison of model results with observations, *J. Geophys. Res.*, *107*(D2), 4013, doi:10.1029/2001JD000410.

Viidanoja, J., V. M. Kerminen, and R. Hillamo (2002), Measuring the size distribution of atmospheric organic and black carbon using impactor sampling coupled with thermal carbon analysis: Method development and uncertainties, *Aerosol Sci. Technol.*, *36*, 607–616.

Virkkula, A., T. Mäkelä, R. Hillamo, T. Yli-Tuomi, A. Hirsikko, K. Hämeri, and I. K. Koponen (2007), A simple procedure for correcting loading effects of aethalometer data, *J. Air Waste Manage. Assoc.*, *57*, 1214–1222, doi:10.3155/1047-3289.57.10.1214.

Vrekoussis, M., E. Liakakou, M. Kocak, N. Kubilay, K. Oikonomou, J. Sciare, and N. Mihalopoulos (2005), Seasonal variability of optical properties of aerosols in the Eastern Mediterranean, *Atmos. Environ.*, *39*, 7083–7094.

Wang, J., et al. (2002), Clear-column radiative closure during ACE-Asia: Comparison of multiwavelength extinction derived from particle size and composition with results from Sun photometry, *J. Geophys. Res.*, *107*(D23), 4688, doi:10.1029/2002JD002465.

Watson, J. G., J. C. Chow, and C. A. Frazier (1999), X-ray fluorescence analysis of ambient air samples, in *Elemental Analysis of Airborne Particles*, edited by S. Landsberger and M. Creatchman, pp. 67–96, Gordon and Breach, Newark, N. J.

Watson, J. G., J. C. Chow, D. H. Lowenthal, C. F. Cahill, D. L. Blumenthal, L. W. Richards, and H. G. Jorge (2001), Aerosol chemical and optical properties during the Mt. Zirkel visibility study, *J. Environ. Qual.*, *30*, 1118–1125.

Weber, R. J., D. Orsini, Y. Daun, Y. N. Lee, P. J. Klotz, and F. Brechtel (2001), A particle-into-liquid collector for rapid measurement of aerosol bulk chemical composition, *Aerosol Sci. Technol.*, *35*, 718–727.

Weingartner, E., H. Saathoff, M. Schnaiter, N. Streit, B. Bitnar, and U. Baltensperger (2003), Absorption of light by soot particles: Determination of the absorption coefficient by means of aethalometers, *J. Aerosol Sci.*, *34*, 1445–1463.

Zhang, X. Q., B. J. Turpin, P. H. McMurry, S. V. Hering, and M. R. Stolzenburg (1994), Mie theory evaluation of species contributions to 1990 wintertime visibility reduction in the Grand Canyon, *J. Air Waste Manage. Assoc.*, *44*, 153–162.

Y. Cai, T. Deshler, and D. C. Montague, Department of Atmospheric Science, University of Wyoming, Laramie, WY 82071, USA. (deshler@uwyo.edu)